Electric properties of dust devils

Gabriele Franzese[1,2], Francesca Esposito[1], Ralph Lorenz[3], Simone Silvestro[1], Ciprian Ionut Popa[1], Roberto Molinaro[1], Fabio Cozzolino[1], Cesare Molfese[1], Laurent Marty[1], Natalia Deniskina[1]

[1]Osservatorio Astronomico di Capodimonte, Istituto Nazionale di Astrofisica, Napoli, Italy; [2]Department of Physics "E. Pancini", University of Naples "Federico II", Napoli, Italy; [3]John Hopkins University Applied Physical Laboratory, 11100 Johns Hopkins Road, Laurel, MD 20723, USA

Keywords:
Dust devils
Dust lifting process
Atmospheric Electricity
Earth
Mars
Meteorology

Abstract

Dust devils are one of the most effective phenomena able to inject dust grains into the atmosphere. On Mars, they play an important role to maintain the haze and can significantly affect the global dust loading, especially outside the dust storm season. Despite dust devils having been studied for a century and a half, many open questions regarding their physics still exist. In particular, the nature

of the dust lifting mechanisms inside the vortices, the development of the induced electric field and the exact contribution to the global atmospheric dust budget are still debated topics. In this paper, we analyze the dust devil activity observed in the Moroccan Sahara desert during a 2014 field campaign. We have acquired the most comprehensive field data set presently available for the dust devils: including meteorological, atmospheric electric field and lifted dust concentration measurements. We focus our attention on the electric field induced by vortices, using this as the principal detection parameter. We present, for the first time, the statistical distribution of dust devil electric field and its relationships with the pressure drop, the horizontal and vertical vortex velocity and the total dust mass lifted. We also compare the pressure drop distribution of our sample with the ones observed on the martian surface showing the similarity of the dust devils samples and the usefulness of this study for the next martian surface missions.

1 Introduction

Dust devils are convective vortices, stable vertical air columns in rotary motion around a low pressure core, able to entrain material from the surface. On Earth, the vortices affect the atmospheric dust concentration of desert areas, but their contribution to the global dust budget is only a few percent (Jemmett-Smith et al., 2015). On Mars, the full impact of dust devils on global dust circulation is not yet fully understood, but is generally considered to be more substantial compared to the Earth (Fenton et al., 2016). By analyzing the dust storms activity on Mars, Guzewich et al. (2015) concluded that they can only explain ~ 50% of the total atmospheric lifted dust. Small scale dust lifting phenomena, in particular dust devils, seem to contribute to the global martian dust budget between 25% and 75%, sustaining the global haze and the concentration of fine aerosol into the atmosphere (Neubauer, 1966; Thomas and Gierasch, 1985; Fedorova et al., 2014).

The first evidence of their existence on Mars was given by the Viking missions (Ryan and Lucich, 1983; Thomas and Gierasch, 1985). In the following years, the presence of dust devils on the planet was largely confirmed and the NASA Mars Global Surveyor and the ESA Mars Express missions allowed the observation from the orbit of dozen dust columns and dust devils tracks (Malin and Edgett, 2001; Greeley et al., 2004; Stanzel et al., 2008). The nearly global Mars coverage of these images showed that dust devils are common and widespread in both hemispheres in every season, almost at every latitudes and elevation. The NASA Pathfinder, Phoenix and Curiosity missions have acquired the meteorological signatures for hundreds of convective vortices (Schofield et al., 1997; Murphy and Nelli, 2002; Ellehoj et al., 2010; Steakley and Murphy, 2016). This was performed by using the atmospheric pressure as principal detection parameter and performing a "phase picker" analysis in order to recognize the drops due to the passage of the vortices low pressure core ("phase picker" is the term used in seismology for event detection – in dust devil analyses it is typically implemented as the detection of a significant negative excursion of a short-period average pressure signal from a long-period average).

However, the pressure is not the only parameter that can easily indicate the passage of dusty vortices. On Earth, sand and dust lifting phenomena are associated with the formation of an induced electric field (E-field). Indeed, during lifting, the individual grains tend to acquire an electric charge by collisions even if the whole dust cloud remains neutral (Kunkel, 1950). On Mars, due to the lack of an adequate in situ instrumentation, the presence of an atmospheric E-field has not yet been confirmed. However, the abundance of entrained dust, the generally favorable condition for lifted grains to acquire and hold charge and laboratory experiments performed in martian like condition, suggest the existence of an atmospheric electric field, widespread across the planet and highly variable in relation to the dust lifting activity (Eden and Vonnegut, 1973; Forward et al., 2009; Barth et al., 2016). The electric field induced by lifted dust may significantly affect the composition of the martian atmosphere and the habitability of the planet, locally enhancing by up to 200 times the chemical formation of oxidants able to scavenge organic material from the surface (Atreya et

al., 2006). Due to the low martian atmospheric electric breakdown field strength (~20 kV/m) (Melnik and Parrot, 1998), the concentration of suspended charges can also lead to the formation of electric discharges that can interfere and cause damage to landed instrumentation, representing an issue for human exploration.

The exact mechanism that leads to grain electrification is still debated and not completely understood (see Harrison et al., 2016 for a review on the topic). For a heterogeneous system the charge acquired during the impacts depends primarily on the composition of colliders (McCarty and Whitesides, 2008), while in a homogenous dust cloud the process seems to be size-dependent: smaller grains tend to charge negatively while larger ones positively (Forward et al. 2009; Lacks and Levandovsky, 2007; Duff and Lacks, 2008; Desch and Cuzzi, 2000; Melnik and Parrot, 1998). Atmospheric convective activity transports grains of different weight to different heights, producing a vertical mass stratification which leads to the charges separation and to the formation of the observed electric field.

The presence of suspended dust negatively charged over a cloud of sand of opposite sign (upward directed E-field) is consistent with the majority of field and laboratory measurements reported in literature (Bo and Zheng, 2013; Frier, 1960; Croizer, 1964 and 1970; Farrell et al., 2004, Jackson et al., 2006). However, there are cases where this electric configuration is not reproduced (Trigwell et al., 2003; Sowinski et al., 2010; Kunkel, 1950) and there are also reported cases where the electric field is downward directed (Demon et al., 1953; Kamra, 1972; Esposito et al., 2016). These works indicate that we are still far from a comprehensive understanding of the E-field development during dust lifting events, motivating the execution of more detailed surveys. Furthermore, few measurements (less than a tenth) of dust devil electric fields have been reported so far (Frier, 1960; Croizer, 1964 and 1970; Farrell et al., 2004; Jackson and Farrell, 2006). These studies present the analysis of isolated events where the E-field is not studied in combination with the meteorological parameters and lifted dust concentration.

In this work we present the analysis of the dust devils activity observed in a field campaign performed in the Moroccan Sahara desert during the 2014 dust storm season. The campaign was carried out in the frame of the DREAMS project, the meteorological station on board of the Schiapparelli lander of the ExoMars 2016 space mission (Esposito et al., 2017). In order to study on Earth the physical processes to be likely encountered on Mars by DREAMS, we deployed a fully equipped meteorological station able also to monitor atmospheric electric field and concentration of lifted sand and dust, acquiring in this way a data set unique in literature. Here, we focus our attention on the electric field induced by the vortices passage, identifying the events using it as principal detection parameter. For the first time, we show the cumulative distribution of the dust induced E-field and we present the relationship between the E-field and the other parameters of the vortices, such as their pressure drop, horizontal and vertical wind speeds and the numeric and mass concentration of lifted dust.

Moreover, we compare the distribution of our sample to the martian dust devils survey showing that the present terrestrial dataset could be useful for studying the dust induced E-field on Mars.

2 Methods

2.1 Equipment

In this work we have analyzed the data acquired during our 2014 field campaign performed in North-Western Sahara Desert of the Tafilalt region (Morocco, 4.110° W, 31.193° N). The site is on the edge of a Quaternary lake sediment bed that is the main source of the measured atmospheric suspended dust. The composition of the sediment (sand, silt, and clay fractions) is the result of the erosion of the regional bedrock of late Paleozoic sedimentary rocks outcropping in the area and is

126 chiefly constituted of detrital shale, quartz, and carbonates grains (see Esposito et al., 2016 for more
127 details).
128 We have monitored a total of 83 days from June 15th to September 5th, using a meteorological
129 station equipped with soil temperature (CS thermistor) and moisture (CS616-C) sensors, three 2D
130 sonic anemometers (Gill WindSonic) placed at 0.5, 1.41, and 4m heights above the ground, one
131 thermometer and humidity sensor (Vaisala HMP155) at 4.5 m and one thermometer (Campbell Sci.
132 (CS)) placed at 2.5 m, one pressure sensor (Vaisala Barocap PTB110) at 2 m, a solar irradiance
133 sensor (LI-COR LI-200 Pyranometer) at 4 m and an atmospheric electric field sensor (CS110) faced
134 down at 2 m. In addition, we have monitored the saltation activity with two sand impact sensors
135 (Sensit Inc.) and three sand catchers (BSNE) placed at different heights (12, 25 and 40 cm) and the
136 atmospheric dust concentration with a sensor (Grimm EDM 164-E) placed at 1.5 m that analyses
137 the dust in 31 channels in the diameter range 0.265- 34 μm. From July 14th we have also added two
138 2D sonic anemometers (Gill WindSonic) placed at 7 and 10 m and one 3D sonic anemometer
139 (Cambell CSAT3) placed at 4.5 m.
140 The station operated 24 hours/day at a sampling rate of 1 Hz, only the 3D sonic anemometer has
141 acquired measures at 20 Hz.
142
143 **2.2 Dust devil structure and identification**
144
145 Fig. 1 shows a dust devil photographed near the measurement site. The diameter of the dust column
146 can remain roughly constant or increase with the height, the column can be perpendicular to the
147 surface or slightly tilted in the direction of motion (Fig. 1).

Fig. 1.

A dust devil observed a few kilometers from the measurement site.

At the center of the column there must be a low pressure core, related to the vertical convection, that induces a horizontal rotary motion of the air flow. The rotational speed is approximately in cyclostrophic balance with the magnitude of the pressure drop ΔP and it can be reasonably described using the Rankine vortex model: the speed linearly increases with the radial distance r from the center of the vortex up to its wall, where it reaches its maximum, then decreases as the reciprocal of r. The pressure has its minimum value in the center of the vortex and the magnitude of the drop decreases with the distance following a Lorentzian curve (Ellehoj et al., 2010). Inside the wall of the column the lifted grains follow an upward helical pattern, forming a debris-laden

159 annulus, while the central region of the vortex is relatively dust free. The vertical wind speed
160 rapidly decreases outside the vertical column, and the dust devil is surrounded by a region
161 characterized by a downward directed motion, where the lifted grains relapse toward the surface.
162 The electrification by collision of the lifted grains and their separation in height induce a dipole
163 configuration of the charges inside the vortex column leading to the generation of an atmospheric
164 electric field (see Murphy et al., 2016 for a review on the subject). Depending on the closest
165 approach distance of the dust devil from the fixed meteorological station (impact parameter) we are
166 able to measure some or all of the characteristics just described. Indeed, we are able to monitor the
167 variation in atmospheric pressure due to ΔP, the peaks in horizontal and vertical wind speed due to
168 the vortex motion, the change in wind direction due to the rotation, the increase in the dust
169 concentration and saltation activity due to the lifted grains, the increase of atmospheric temperature
170 related to the lifting of the near ground air layers and the variation in atmospheric electric field due
171 to charged grains. Moreover, we are able to measure the decrease in solar radiation if the shadow
172 due to the dust column covers the station.
173 The evaluation of the impact parameter from the data acquired by a fixed meteorological station is
174 not a straightforward procedure. Recently, Lorenz (2016) has proposed a model to estimate this
175 parameter, however, the process entails some ambiguities and we have decided to not attempt this
176 kind of analysis in the present work. Nonetheless, we can easily recognize if an event passes over
177 the meteorological station by the peculiar features of the signal. Let us define the impact parameter
178 as the closest approach distance between the center of the vortex and our instruments. Fig. 2
179 schematically shows the passage of two dust devils: the first one does not intercept the
180 meteorological station (Fig. 2a), the second crosses the instruments (Fig. 2b). In the case depicted in
181 Fig. 2a we measure a single maximum in the variation of all the monitored parameters in the instant
182 t_1, corresponding to the maximum approach of the vortex to the station. Instead, when the impact
183 parameter is smaller than the radius of the dust devil, the vortex wall passes two times over the
184 station (time instants t_0 and t_2 of Fig. 2b). In these instants the instruments measure the maximum

values of horizontal and vertical wind speed, lifted sand and dust concentration and hence E-field variation. Between t_0 and t_2 the dust-free inner part of the vortex crosses the station resulting in a decreasing of the magnitude of the wind speed and grains concentration, that reach the local minimum in the instant t_0. For the pressure signal, taking into account that the magnitude of the pressure drop ΔP is maximum in the center of the vortex and not on the wall, we measure a single maximum of ΔP in the instant t_1 in both cases of Fig. 2a and Fig. 2b. We are then able to distinguish between the case of Fig. 2a and Fig. 2b by looking for a single or a double peak trend in the measured data of wind speed, grains concentration and E-field. The double peak feature is usually particularly marked in the horizontal wind speed data, becoming clearer also in the other affected parameters when the impact parameter approaches zero.

We report the magnitude of the monitored parameters inside the dust devils as the values assumed: in t_1 for the Fig. 2a case, and in the higher of the two maxima for parameters affected by the double peak trend for the Fig. 2b case.

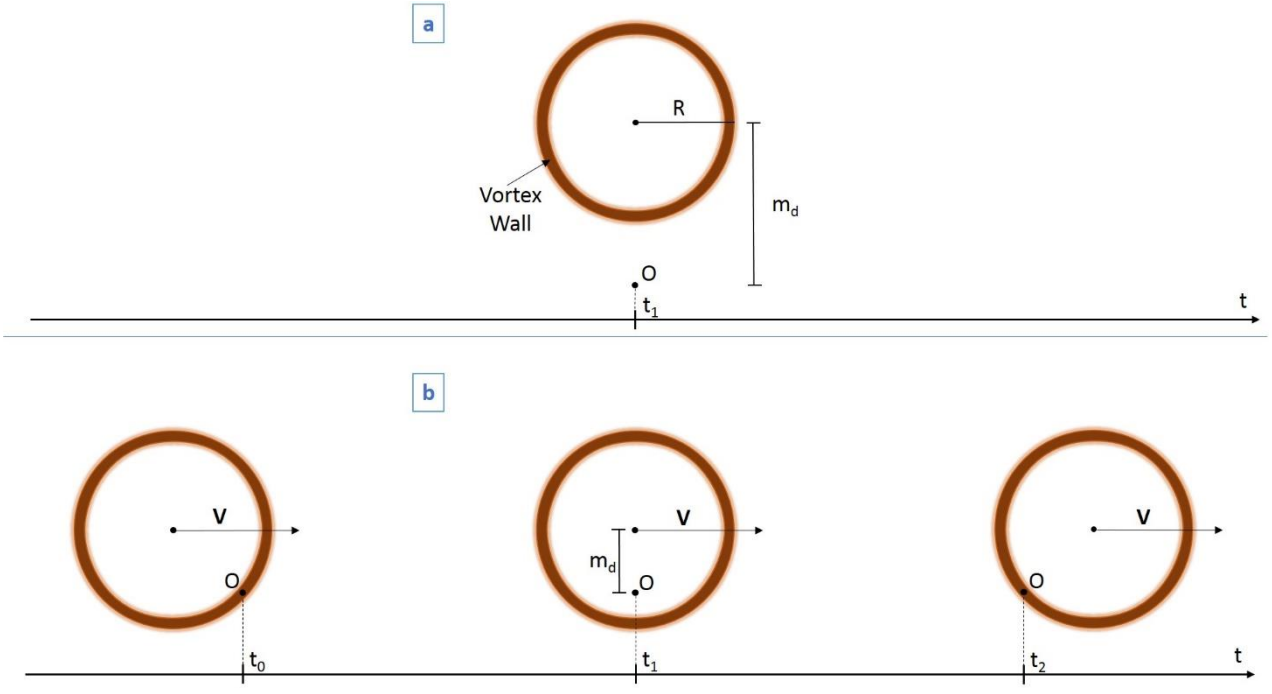

Fig. 2.

(a) A dust devil of radius R that passes out of the meteorological station placed at the point O. t_0 represents the instant of maximum approach m_d to the station. (b) A dust devil that intercepts the meteorological station seen in three different instants. The vector ***V*** *represents the translational velocity of the vortex. t_0 represents the instant when the vortex wall passes over the station the first*

time, t_1 represents the instant when the vortex center reaches its maximum approach to the station and t_2 represents the instant when the dust devil moves away crossing for the second time the station with its wall.

2.3 Dust devils detection algorithm

The signatures related to the dust devil passage last from few seconds to a couple of minutes. The vortices encounters are usually identified by performing a "phase picker" analysis on the recorded pressure time series (Murphy and Nelli, 2002; Ellehoj et al., 2010; Steakley and Murphy, 2016; Lorenz and Lanagan, 2014). The phase picker compares a long term estimator of the pressure with a short term one to recognize the fast variation of the signal. In order to identify even the shortest encounters, we have chosen to compare the twelve minutes median of the signal with the 1 Hz rate measurements. Unlike the previous literature works, we have chosen to use the electric field instead of the pressure as the principal detection parameter. Indeed, the vortex pressure drop ranges from few tents of mbar to a couple of mbar, while the standard deviation along the twelve minutes' pressure median is ~0.1 mbar. Instead, the vortex induced E-field ranges from few hundreds of V/m up to twenty thousand V/m, while the deviation around the twelve minutes' median is only few V/m. For this reason, the E-field variation is the most easily recognizable feature associated with the dust devil passage.

Our algorithm splits the whole day in time intervals of 12 minutes each and selects as "Class D" events the ones for which: $|E - E_m| \geq E_l$, where E_m is the median E-field, E is the 1 Hz measurement and E_l is the chosen threshold. The detection of a single dust devil feature, e.g. only the E-field variation, is not enough to unambiguously recognize the event. This is because we need the synchronous detection of other vortex distinctive characteristics in order to proper distinguish between a dust devil and other kind of dust lifting phenomena. As an example, a gust could exhibit a similar E-field variation but not the same trend of pressure drop and change in wind direction. Hence, the next step of the algorithm analyses the wind direction and the pressure time series of

each Class D event. For the pressure we have chosen to perform an 11 seconds running average in order to reduce the rather high noise of our sensor. When the pressure drop (ΔP) and wind direction variation (ΔWd) overcome the chosen thresholds P_l and Wd_l respectively, the events are categorized as "Class C".

We used the following thresholds: E_l=250V/m, P_l=0.18 hPa, Wd_l=25°. The threshold values have been chosen analyzing a subset of the whole dust devils sample, studying the typical magnitude of the induced variation and the noise level. In order to eliminate the false-positive detections (mainly gusts and pieces of dust storms), the Class C events have been cross-checked using the other measured parameters as the horizontal and vertical wind speed, lifted sand and dust concentration, solar radiance and atmospheric temperature. We categorized as Class B events the ones with a clear dust devil signature in all the parameters, except the pressure drop, whose magnitude could remain partially hidden by the noise. When also the pressure shows a clear vortex trend the event is categorized as Class A.

The Class A detections represent roughly a quarter of the Class C and one half of the Class B events and they are the only ones considered and analyzed in the present work.

2.4 Evaluation of the vortex wind speed and the concentration of the lifted mass

Let us call vortex wind speed (v_w) the relative horizontal speed of the dust devil in the rest frame of the background wind ($\boldsymbol{b}$). We directly measure the total wind speed $\boldsymbol{v_t} = \boldsymbol{v_w} + \boldsymbol{b}$. The point of minimum distance of the dust devil from the meteorological station corresponds to the maximum measured velocity. In order to estimate v_w in this point we can consider the relation: $\boldsymbol{v_w} = \boldsymbol{v_M} - \boldsymbol{b}$, where v_M is the maximum of v_t measured during the dust devil encounter, while b is the median background wind speed on a time interval of twelve minutes around the events. We have evaluated all the quantities using the data acquired by the anemometer placed at 4 m.

The dust size fraction of the soil in the site of measurements is composed mainly of quartz (ρ=2.66 g/cm^3) and muscovite (ρ=2.82 g/cm^3), with a minor part of calcite (ρ=2.71 g/cm^3) and illite (ρ=2.79 g/cm^3) (Esposito et al., 2016). Its density can be roughly estimated as ρ_t=2.7 g/cm^3. We have evaluated the total lifted mass density of dust (with diameter $\leq$ 34 μm) using the direct measurement of the dust grains numeric concentration and size distribution and assuming ρ_t as the mean density.

3 Results

We observed a total of 556 Class A dust devil's passages during 83 days of measurements. For 338 of these we also collected their vertical wind speed (only 54 days are comprehensive of the 3D anemometer measurements). The values of the measured parameters for all the Class A events are presented in Supplementary Table 1.

Fig. 3 shows an example of sensors' response to one of the events. In this instance, all the dust devil features previously described are clearly recognizable. In Fig. 3a we can see the drop due to the vortex low pressure core, Fig. 3b shows the E-field peak due to the passage of the charged grains, Fig. 3c shows the increase in saltation activity measured by the Sensit and Fig. 3d the increase in temperature related to the convection lifting of the warm air layer near the ground. In Fig. 3e we show the peak in vertical wind speed connected with the upward motion inside the vortex column (negative values indicate a downward directed velocity). The rotational motion of the vortex it is added to the motion of the wind background. Hence, during the passage of the dust devil the measured wind speed will increase proportionally to the magnitude of the rotational speed (Fig. 3f) and the direction of the wind will change accordingly to the rotation (Fig. 3g). Finally, Fig. 3h and Fig. 3i show the peak in the lifted dust concentration and the decrease in the measured solar radiance due to the passage of the dust column and its shadow.

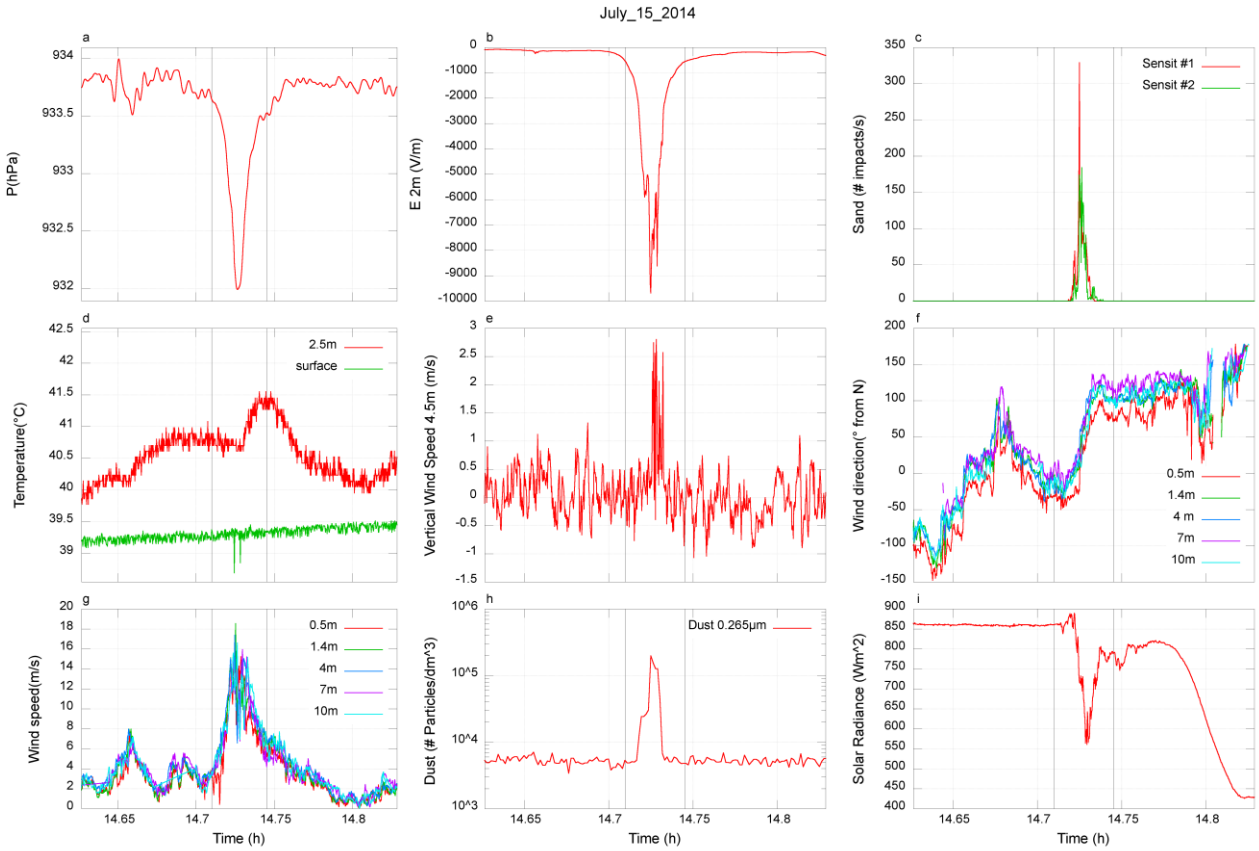

Fig. 3.

A dust devil (Class A) encounter as detected by our measurement station. The plots show the time series of the different monitored parameters. In order from left to right and from top to bottom there are: (a) atmospheric pressure, (b) E-field, (c) counts of near surface saltating grains, (d) temperature, (e) vertical wind speed, (f) horizontal wind direction, (g) horizontal wind speed, (h) lifted dust concentration and (i) solar radiance.

Fig. 4 shows a zoom of the same event where, in order to make the figure as clear as possible, we have plotted only the time series of the wind speed measured at 4 m and of the pressure. It is possible to recognize how the wind speed shows a double peak trend. The two maxima are located at the time instant t_0 and t_2, they precede and follow the maximum pressure drop located at t_1, which is synchronized with a local minimum in the wind speed. This particular trend reflects the case described in Fig. 2b, indicating the passage of the vortex directly over our meteorological station. The individuation of the exact position of the instants t_0, t_1 and t_2 can result tricky, because it depends on the wall thickness of vortex, its motion and fluctuation speed level. For example, in the specific case of Fig. 4, t_0 and t_2 are not evenly spaced from t_1 and we observe two different

maximum values. This is probably due to a small deviation of the vortex from the uniform linear motion, suggested also by the slight asymmetry of the pressure drop. Anyway, we are not interested in the evaluation of the peculiar position of these instants, but just to the individuation of the two peaks signal trends to obtain information on the vortices that crossed or not our instruments.

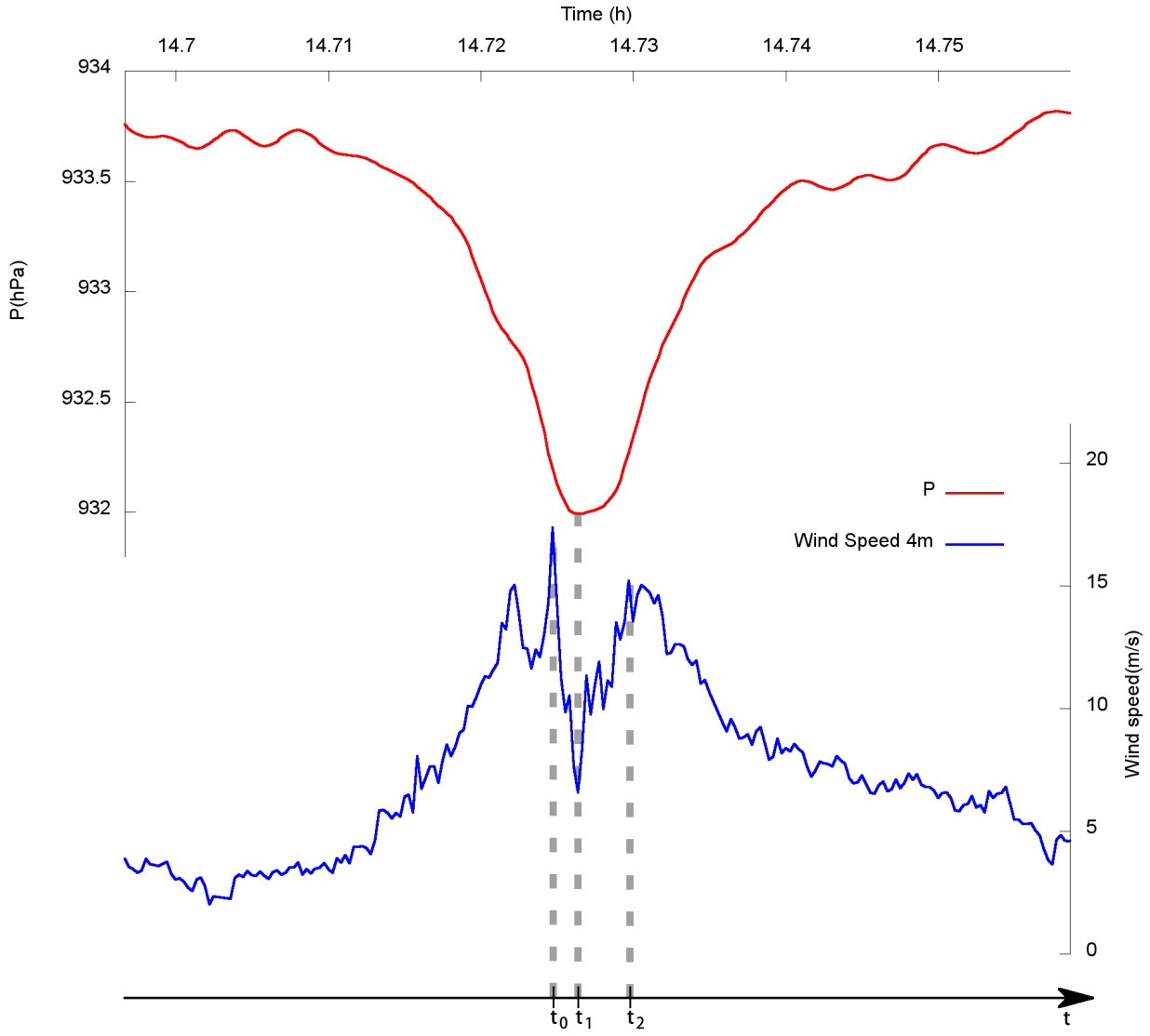

Fig. 4.

Time series of the atmospheric pressure and horizontal wind speed of the events of Fig. 3. The single peak trend of the pressure and the double peak trend of the wind speed are clearly recognizable indicating the direct passage of the dust devil over the station. The time instant t_0 and t_2 represent the first and the second crossing of the vortex wall, while t_1 is the maximum approach point, as described in Fig. 2b.

In Fig. 5 we take a close look to the recorded vertical E-field, pressure drop and lifted dust for three different events with a strong, medium and tiny atmospheric E-field variation, respectively. This signatures are always well visible and distinct from the background and the pressure signature appears to last for a longer time than the corresponding E-field variation. The E-field signature is usually roughly symmetric, however strongly asymmetric events as the one depicted in Fig. 5c are not totally uncommon. In particular, during the passages over the station, we observed both single and double peaks shape as well as irregular and highly noise signals. We do not to speculate on the meaning of these trends, because of the high number of possibilities coupled with low statistics for each case.

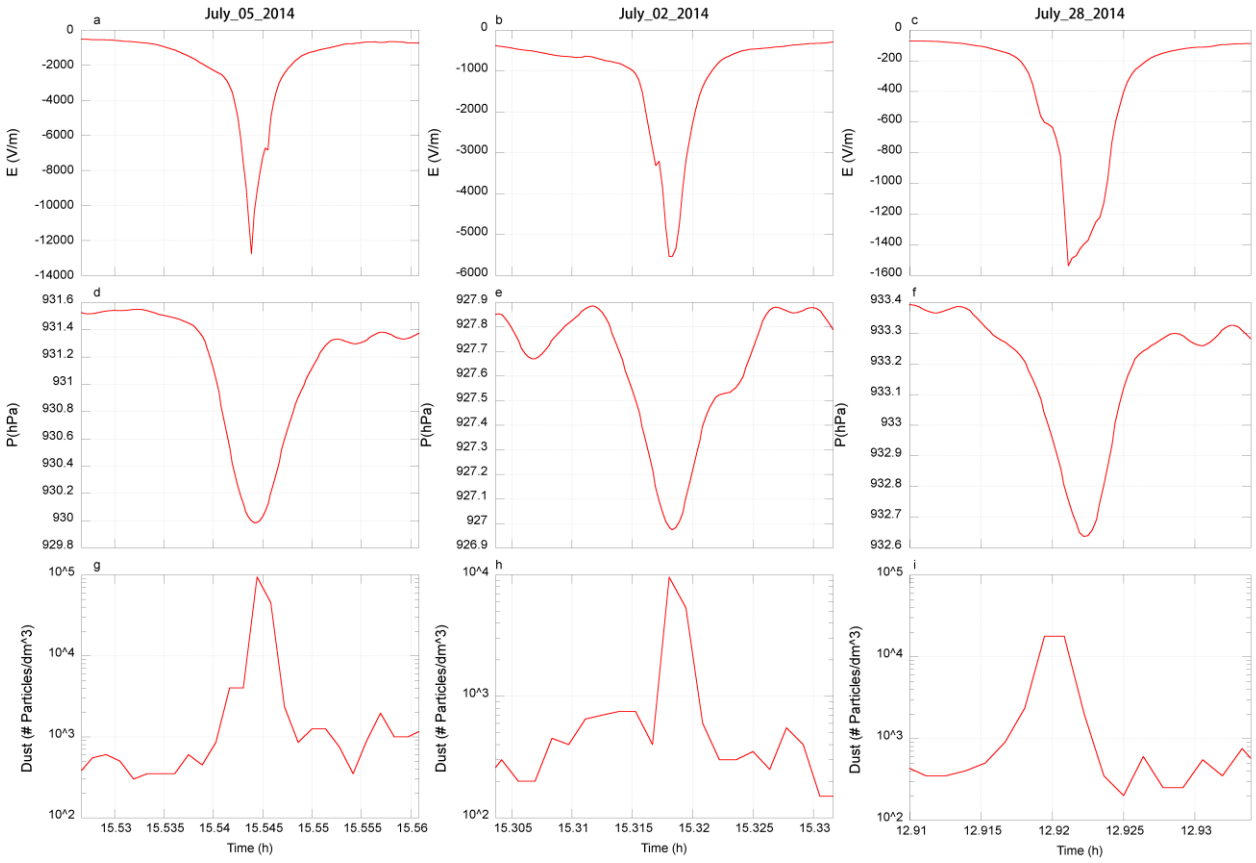

Fig. 5. The vertical E-field time series for three Class A events of strong (a), medium (b) and tiny (c) magnitude, respectively. For the same events there are also reported the pressure drops (d, e, f) and the dust concentration in the bin-size 1.45µm (g, h, i).

Most of the dust devil events described in this study are coupled with moderate wind speeds (~ 6 m/s) from the SW, which is the typical wind regime observed during the campaign. Fig. 6 shows the distributions of the vortex wind speed, vertical upward wind speed, pressure drop, and absolute

E-field observed during the dust devils encounters. The vortex wind speed ranges from 2.3 m/s to ~ 17.5 m/s, with a mean value of ~ 6 m/s (Fig. 6a). The vertical wind speed ranges from 0.1 m/s to 5 m/s, with a mean value of ~ 1 m/s (Fig. 6b). Even when the vortices pass exactly over our station the maximum vertical wind speed remains ~ 1.5 m/s and only during two events it overcomes 3 m/s. We observed that the dust devil passage leaves a signal clearly recognizable in horizontal wind speed and direction, pressure and E-field time series, with a full duration half maximum of various seconds. Compared to these ones, the trace left in the vertical wind speed is usually more similar to a delta function or a series of deltas, without a clear trend of growth and decrease in time (see for example the Fig. 3e). The reduced duration of the vertical flow signal coupled with its tiny magnitude makes the vertical wind speed peak less clear to recognize and study than the other dust devils features. This led us to the conclusion that the upward and downward vortex air flows have to decay much faster with the distance than the other monitored parameters.

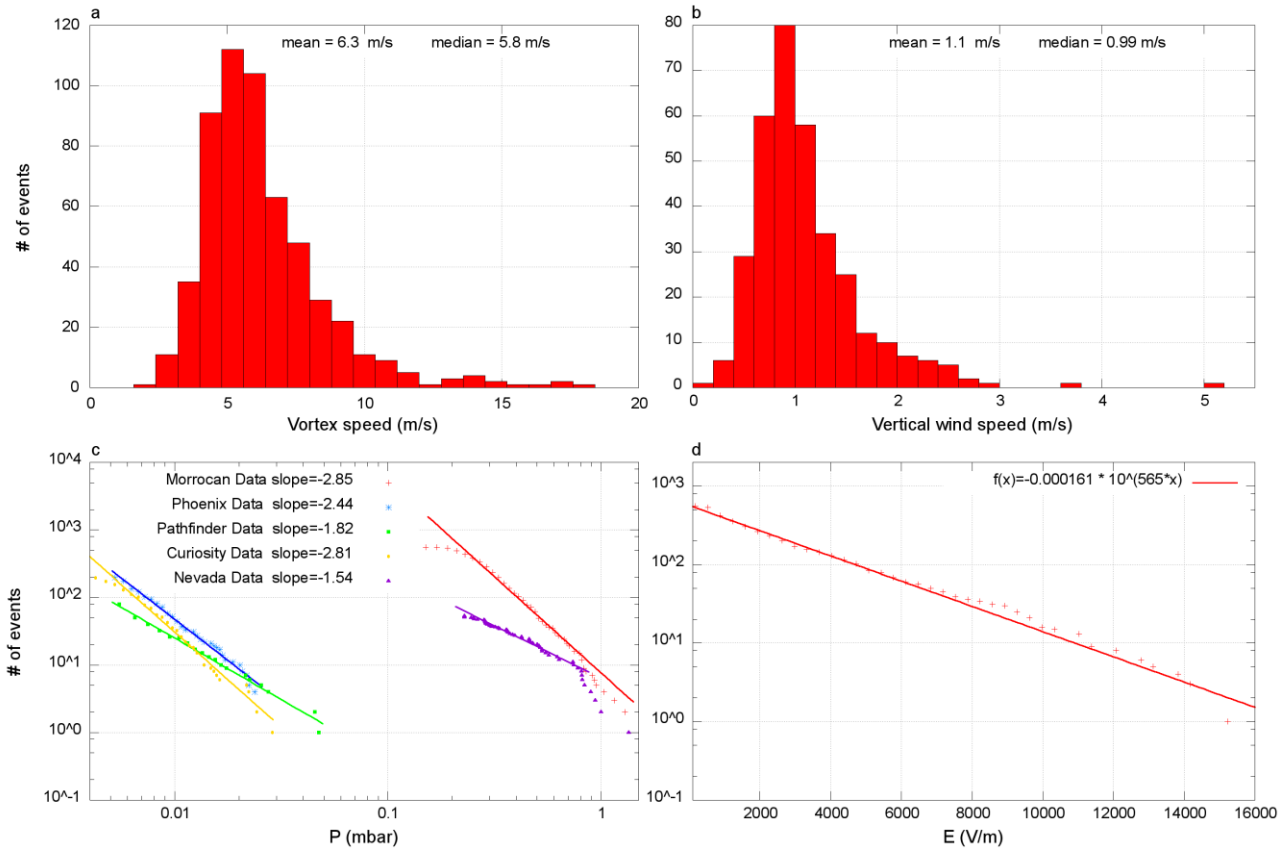

Fig. 6.

(a) Histogram of the vortex wind speed; (b) Histogram of the maximum vertical wind speed;

(c) Cumulative distribution of the pressure drop for our data set (red) and for comparison a survey taken in Nevada (Category 1 events in the P28 dataset of Lorenz and Lanagan, 2014 – violet), the dust devils seen by the Phoenix (blue), the Pathfinder (green) and the Curiosity (yellow) missions. The straight lines are the respective best fit functions.

(d) Cumulative distribution of the maximum electric field (red) in a semi-log plot with the best fit line (solid line).

The measured pressure drops (ΔP) range from 0.18 (the chosen threshold) to 1.3 hPa (in red in Fig. 6c). Most of the detected vortices lie in the range 0.2-0.8 hPa and in this interval the ΔP cumulative distribution is well described by a power law ($y = a\ x^b$ with and exponent b = -2.85 ± 0.05). For the largest and smallest ΔP values an appreciable drop off from the power law is apparent, as also seen in other terrestrial data (e.g. in Fig. 6c we shown a dataset from Lorenz and Lanagan, 2014). However, we observed that in the same range 0.2-0.8 hPa the ΔP cumulative distribution can be also described by an exponential function with a coefficient of determination comparable to the one of the power law fit ($y = a\ 10^{b\,x}$ with an exponent b = -3.32 ± 0.05). Although there is not a compelling reason to prefer one representation to another, throughout this paper we will continue to use the results of the fit power law in order to allow an easier comparison with the literature.

Fig. 6c also shows a comparison of our data with the martian convective vortices survey obtained by the Pathfinder and Phoenix landers and by the Curiosity rover, where a similar power law cumulative distribution is observed (Murphy and Nelli, 2002; Ellehoj et al., 2010; Steakley and Murphy, 2016). The exponent of the power law (-2.81 ± 0.07) that describes the vortex pressure drops observed by Curiosity is compatible with the one obtained for our Moroccan data (-2.85 ± 0.05).

Fig. 6d shows in a semi-log plot the cumulative distribution of the absolute E-field values measured during the dust devils encounters. The vertical induced E-field is always downward directed and it usually differs from the fair weather value (~-50 V/m) of few thousands V/m, reaching values up to 16000 V/m. The cumulative distribution is well described in the whole variation range by an exponential law, $y = a\ 10^{b\,x}$ with exponent of (-161 ± 4) $\cdot 10^{-6}$ $(V/m)^{-1}$.

Fig. 7 shows the relations between the dust devils E-field and the other meteorological parameters. The E-field variations show an approximatively linear relation with the pressure drop (Fig. 7a), the vortex wind speed (Fig. 7b), and with both the upward and the downward directed vertical wind speed (Fig. 7c and Fig. 7d).

Fig. 8 shows the relation between the E-field and the amount of lifted dust. In Fig. 8a we plotted the lifted dust grains concentration against the corresponding E-field absolute value. In red are shown the data related to the dust devils and for comparison in blue there are data related to the dust storms observed during the same field campaign. We found that the dust concentration and the induced E-field are related by a linear function for both the dust devils and the dust storms and the slopes are compatible (dust devils slope = $(3.7 \pm 0.2) \cdot 10^2$ $dm^{-3}(V/m)^{-1}$, dust storms slope = $(4.0 \pm 0.3) \cdot 10^2$ $dm^{-3}(V/m)^{-1}$). Finally, Fig. 8b shows in a semi-log plot that the relation between the E-field magnitude and the lifted mass concentration can be described by a power law (exponent = 0.53 ± 0.05).

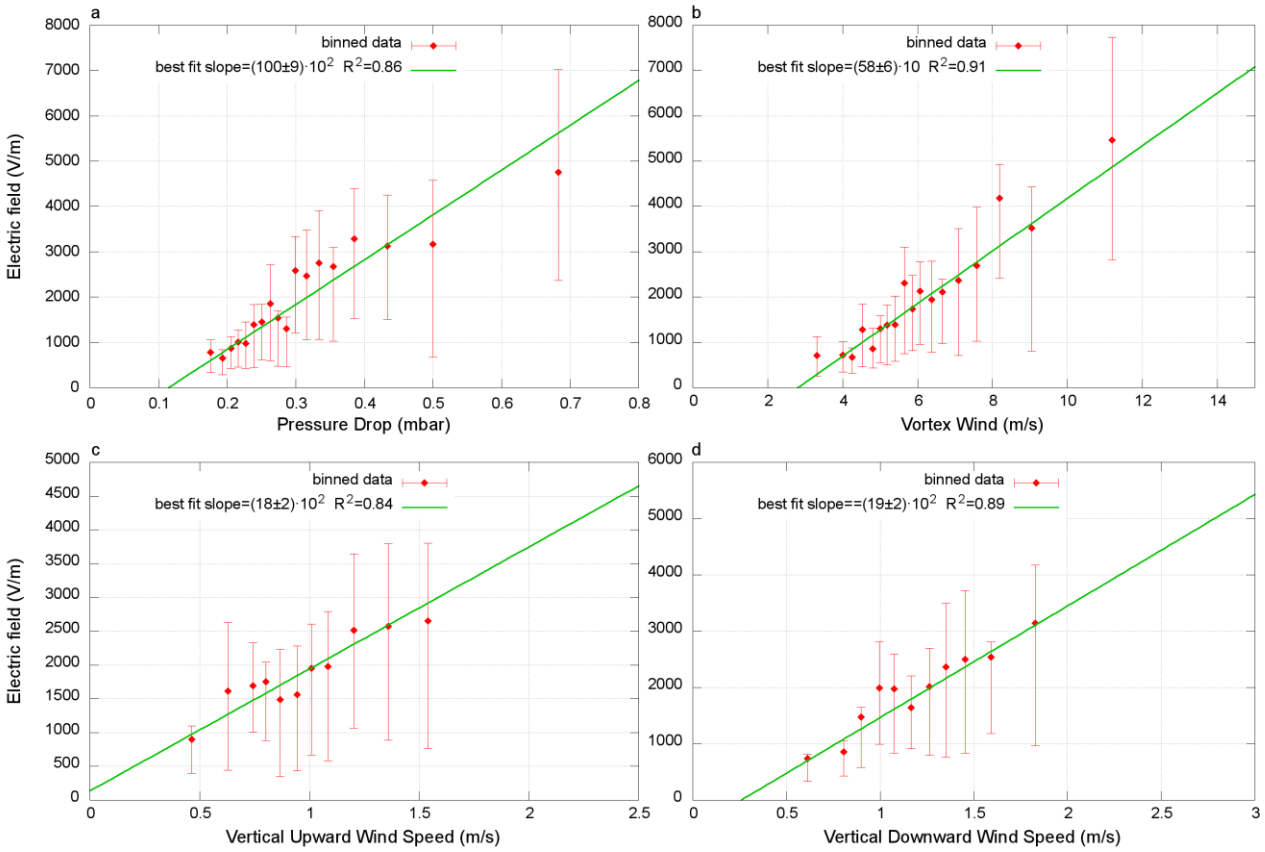

Fig. 7.

Relation between the dust devils E-field and:

(a) the pressure drop, best fit slope=(100 ± 9)·10^2 (Pa)$^{-1}$ V/m R^2= 0.86; (b) the vortex wind speed, best fit slope=(58 ± 6)·10 (m/s)$^{-1}$ V/m R^2= 0.91; (c) the upward vertical wind speed, best fit slope=(18 ± 2)·10^2 (m/s)$^{-1}$ V/m R^2= 0.84; (d) the downward vertical wind speed, best fit slope=(19 ± 2)·10^2 (m/s)$^{-1}$ V/m R^2= 0.89. Each point in a) and b) represents a bin of 30 dust devils, in c) and d) due to the lower statistic we used a bin of 28 dust devils; the error bars represent the 25th and 75th percentile.

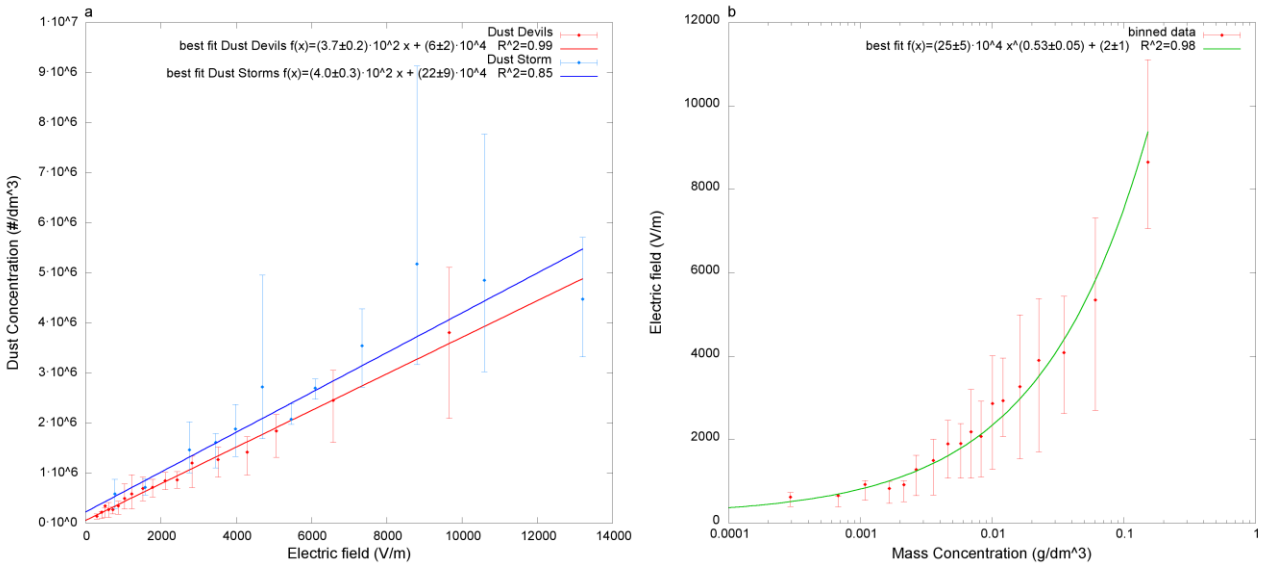

Fig. 8.

a) the total dust grain concentration is shown as a function of the induced E-field for the dust devils (in red) and the dust storm (in blue) events observed during the field campaign. (b) Semi-log plot that shows the relation between the induced E-field and the total dust mass concentration during the dust devils events. Each point represents a bin of 30 events for the dust devils and of 7 events for the dust storms; the error bars represent the 25th and 75th percentile.

4 Discussion

4.1 Wind speed distribution

Reporting the results of the field campaigns he performed in Arizona, Sinclair (1973) observed how the vertical wind speed of the vortices measured approximatively at 2.1 m and 9.4 m usually reaches 10 m/s inside the dust column, rapidly decreasing outside it. The vertical speeds we measured at 4.5 m are far slower than the ones observed by Sinclair, even for the vortices that pass exactly over our station (Fig. 6b). We also noted that the measured vortex horizontal wind speeds

usually overcome the vertical speeds. This result is in agreement with the observations made by Ryan and Carroll (1970), which reported vertical wind speeds measured at 2 m from ground between 0.2 m/s and 2.2 m/s, approximately one order of magnitude lower than the horizontal wind speed. Hence, taking into account the typical values of vertical and horizontal wind regime observed during our events, we can estimate that even for dust-size grains the contribution to the lifting due to the horizontal wind stress is not negligible compared with the force due to the vertical flow.

4.2 Relation between the E-field and the pressure drop

Greeley et al. (2003) observed how the dust devils can entrain dust with wind speed up to 80% lower than the ones required by the simple boundary layer winds. This feature may derive from the presence of the pressure gradient force due to the vortex low pressure core, that acts like an additional lifting force (Neakrase et al., 2016). The magnitude of the pressure drop is therefore related to the amount of the lifted dust that generate the E-field. Lorenz et al. (2016) present some indications of a correlation between the vortex ΔP and the induced vertical electric current. Our data show for the first time that the induced E-field and the vortex ΔP are actually connected, and that the relation is approximatively describable by a linear function (Fig. 7a). A possible explanation for the large error bars shown in Fig. 7a is the different dependence of plotted quantities on the distance between the vortex and the station (impact parameter) and the impossibility to unambiguously infer this parameter from the measurements acquired by a fixed meteorological station.

Indeed, the ΔP magnitude decreases like the square of the impact parameter (Ellehoj et al., 2010), while the E-field decreases like the third power of the distance (assuming a dipole configuration). This different dependence is noticeable also in our data. Indeed, we observed how the full width half maximum of signal induced by the vortex passage is around 50% longer in the pressure time series than in the E-field one, see for example Fig. 5 for a comparison of the two signal duration.

Moreover, we have to consider that also the vortex diameter could not be directly inferred from our data. Currently it is not known how the magnitude of the induced E-field depends on the vortex size, hence, a different dependence on the diameter of the two quantities plotted in Fig. 7a could not be excluded and could lead to a further increase of the uncertain. These last considerations can also be extended the other reported comparisons between the vortex parameters, and we believe that the indetermination on impact parameter and vortex size represents the main source of error for each relation shown in Fig. 7 and Fig. 8. A new field campaign with synchronous measurements of the electric, meteorological and morphological vortex parameters has already been planned by the authors in order to resolve the degeneration that currently affect the data and further investigate this subject.

4.3 E-field orientation and its relation with the wind speed

Farrell et al. (2006) modelled the electric field generated by a dust devil system composed by grains of two sizes stratified by gravity, assuming that the small and the large ones tend to acquire a negative and a positive charge respectively (E-field upward directed). Moreover, they assumed the horizontal wind contribution to the lifting process to be negligible compared to the vertical one. In Fig. 7 of their paper, the authors showed how the modelled vertical E-field is linearly related to the upward vertical wind speed. Nonetheless, they pointed out that this relation has to be applied with caution to the case of vertical speed whose magnitude is small enough to be compared with the horizontal one, because this possibility is not contemplated in their model.

Actually, according to our data, the E-field and the vertical wind speed seems to be linearly related and the relation subsists also for the low upward vertical wind speed (Fig. 7c). Differently to the assumption of Farrell et al. (2006), we see that the contribution of the horizontal wind is not negligible, indeed, a relation between and the E-field and v_w exists (Fig. 7b).

445 Moreover, we have observed that the induced E-field seems to be also related to the downward
446 directed wind component (Fig. 7d). This downward motion is usually predominant right outside the
447 dust column, where the grains start to sediment by convective flow motion and gravity. This
448 suggests that the electric current related to the descending motion of the grains could play an
449 important role on the behavior of the E field, while, currently the dust devils E-field models don't
450 take into account this contribution (Farrell et al., 2006, Barth, 2016).
451 An important difference between our results and those commonly reported in the dust devil's
452 literature is represented by the orientation of the vertical E-field. The charges configuration inside
453 the dust column is usually described as an electric dipole with the positive charges below and the
454 negative ones above, leading to an upward directed vertical E-field (Farrell et al., 2006; Barth et al.,
455 2016). This assumption is in agreement with the previous field measurements of dust devils E-field
456 (Freier, 1960; Crozier, 1964; Farrell et al., 2004; Jackson et al., 2006). As far as we know, our data
457 set is the first example of a dust devils sample entirely characterized by a downward directed E-
458 field. This could be a first evidence that the orientation of the E-field induced by dust devil is not a
459 universal property but is a variable that may depend on local atmospheric conditions and soil
460 composition, as observed e.g. by Kamra 1972 for the dust storms.
461 The comprehension of this subject require further investigation, in particular laboratory analysis on
462 the composition and size distribution of the soil that sustain the whirlwinds.
463

464 **4.4 The E-field in other dust lifting processes**

465

466 Esposito et al. (2016) showed that during the dust storms the vertical E-field is linearly related to
467 the lifted grains concentration.
468 Here, in the place of the instant by instant values considered by Esposito et al. (2016), we have
469 analyzed the maximum of grains concentration vs maximum induced E-field intensity for both dust
470 devils and dust storms events (Fig. 8). We have observed that the E-field (E) and the grains numeric

concentration (η) are linearly related also during the dust devil events, and even that the slope of the relation is compatible with the dust storms one. This correspondence indicates that the linear relation E-field/grain concentration is probably a general law common for the dust lifting phenomena.

Assuming a dipole model with the charges uniformly distributed inside the walls of a cave cylinder, starting from the E/η relation we can suppose on a first approximation a direct linear relation between space charge density ρ and η. We have applied this simple model to the vortices passing over the station, roughly estimating their size from the passage duration and travelling speed. With these parameters, we can estimate the average charge per grain (q) and the charge density ρ for these events. We have found a value of q ranging between $8 \cdot 10^{-18}$ and $5 \cdot 10^{-17}$ C, in agreement with what reported by Kunkel 1950, and a value of ρ between $3 \cdot 10^{-9}$ and $4 \cdot 10^{-8}$ C/m^3.

Using these values of q and scaling the other parameters to the ones expected during dust devils on Mars: an η around hundreds of grains for cm^3 and a vortex diameter between 2 and 276 m (Greeley et al. 2010); we obtain a value of E ranging from few hundreds of V/m up to over 35 kV/m. Hence, supposing a similar value of charge per grains on Earth and Mars, there is the possibility to overcome the value expected for the martian electric breakdown, as firstly supposed using laboratory measurements by Eden and Vonnegut 1973 and recently repurposed by the work of Farrell et al. 2017.

4.5 Comparison with martian data

Previous convective vortex studies have observed how, for both terrestrial and martian surveys, the ΔP cumulative distribution appears to be well described by a power law function. In some cases, the distribution of the smallest and largest ΔP does not follow the main trend (Steakley and Murphy, 2016; Lorenz and Lanagan, 2014). This deviation could be attributable to the inefficient detection of the smallest vortices and to the under sampling of the largest ones due to the finite sample size

(Jackson and Lorenz, 2015). However, a reason of physical nature cannot be excluded. Our results are generally in agreement with the literature, but the value of our power law exponent (-2.85) differs from the ones previously reported in other dust devil terrestrial surveys (~-1.5). Our power law exponent approaches the one observed on Mars during the Phoenix (-2.44) and Curiosity (-2.81) missions, resulting compatible with this last one (Fig. 6c). The exact exponent value and uncertain evaluated through the regression process are strictly related to the chosen ΔP range and binning procedure (see e.g. Lorenz and Jackson, 2016), thus a precise comparison of the different surveys is not possible. However, it is clear that the terrestrial and the martian convective vortices distribution show many similarities, allowing to speculate that our results on the induced E-field could be representative also of the martian dust devils.

5 Summary and conclusions

In preparation to the ExoMars 2016 Schiaparelli mission, we have performed a field test campaign in the Moroccan Sahara Desert. We deployed a fully equipped meteorological station, also able to measure the vertical atmospheric electric field and the lifted dust concentration. We monitored three months of dust devils activity and we observed how the variation in atmospheric electric field induced by the dust devil passages represents the clearest and easiest feature to recognize. On this basis, we used the vertical E-field as the principal probe parameter to detect the dust devils' passage. We identified 556 events, acquiring a data set unique in literature with synchronous measurements of the meteorological parameters, atmospheric electric field and dust concentration. These data represent up to now the most comprehensive survey available for the convective vortices and they allow the first statistical study of the dust devils induced electric field. The data set is entirely characterized by a downward directed E-field, whose cumulative distribution is well described by an exponential law. The E-field orientation is opposite to that reported in literature for

previous dust devils measurements suggesting a charge distribution in the dust column not contemplated in the current dust devil E-field model (Barth et al., 2016).

We observed how the induced E-field appears to be related to the other vortex parameters: it is linearly related to the vortices pressure drop and horizontal wind speed, to both the upward and downward maximum vertical wind speed observed during the events and to the numeric concentration of dust lifted grains. In addition, the E-field is related by a power law to the lifted dust mass concentration. In particular, we observed that the dust storms and the dust devils present the same correlation between the induced E-field and the amount of lifted grains, suggesting the existence of a general law common to different kinds of dust lifting events.

We compared our vortex pressure drop distribution with the one obtained for the martian surveys. In analogy to Mars the ΔP cumulative distribution follows a power law function with an exponent compatible with the one observed by NASA Curiosity mission (Steakley and Murphy, 2016). The similarity between the dust devils distribution in the two planets emphasizes the usefulness of our work for the understanding of the martian dust lifting phenomena. The study of the martian atmospheric electromagnetic field in dusty environment is one of the objectives of the ExoMars 2020 mission. The surface platform of the mission has on board the “Dust suite”, a package of sensors able to monitor the lifted dust size distribution, concentration and atmospheric electric field, that will acquire data similar to the ones collected in Morocco. The present study on the dust induced E-field on Earth is a fundamental preparation to the analysis of the martian measurements, providing also the best comparative data available at moment.

Acknowledgments

This work has been supported by the Italian Space Agency through the agreement I/018/12/0: "DREAMS EDM Payload—ExoMars 2016", and, in part by the Istituto Nazionale di Astrofisica (INAF). The development of DREAMS instrument is funded and coordinated by ASI under the leadership of INAF-Naples, Italy.

References

1. Atreya, S. K., Wong, A. S., Renno, N. O., Farrell, W. M., Delory, G. T., Sentman, D. D., ... & Catling, D. C. (2006). Oxidant enhancement in martian dust devils and storms: implications for life and habitability. *Astrobiology*, *6*(3), 439-450.

2. Barth, E. L., Farrell, W. M., & Rafkin, S. C. (2016). Electric field generation in Martian dust devils. *Icarus*, *268*, 253-265.

3. Bo, T. L., & Zheng, X. J. (2013). A field observational study of electrification within a dust storm in Minqin, China. *Aeolian Research*, *8*, 39-47.

4. Crozier, W.D. (1964), The electric field of a New Mexico dust devil, J. Geophys. Res 69, 5427, 1964. doi: 10.1029/JZ069i024p05427.

5. Crozier, W. D. (1970), Dust devil properties, J. Geophys. Res., 75, 4583–4585.

6. Demon, L., DeFelice, P., Gondet, H., Kast, Y., & Pontier, L. (1953). Premiers résultats obtenus au cours du printemps 1953. *J. Rech. Cent. Natl Rech. Sci*, *24*, 126-137.

7. Desch, S. J., & Cuzzi, J. N. (2000). The generation of lightning in the solar nebula. *Icarus*, *143*(1), 87-105.

8. Duff, N., & Lacks, D. J. (2008). Particle dynamics simulations of triboelectric charging in granular insulator systems. *Journal of Electrostatics*, *66*(1), 51-57.

9. Eden, H. F., & Vonnegut, B. (1973). Electrical breakdown caused by dust motion in low-pressure atmospheres: Considerations for Mars. *Science*, *180*(4089), 962-963.

10. Ellehoj, M. D., Gunnlaugsson, H. P., Taylor, P. A., Kahanpää, H., Bean, K. M., Cantor, B. A., ... & Holstein-Rathlou, C. (2010). Convective vortices and dust devils at the Phoenix Mars mission landing site. *Journal of Geophysical Research: Planets*, *115*(E4).

11. Esposito, F., Molinaro, R., Popa, C. I., Molfese, C., Cozzolino, F., Marty, L., ... & Ori, G. G. (2016). The role of the atmospheric electric field in the dust-lifting process. *Geophysical Research Letters*, *43*(10), 5501-5508.

12. Esposito et al. 2017 The DREAMS experiment onboard the Schiaparelli Module of the ExoMars 2016 mission: design, performances and expected results, *Space Science Reviews*, under review

13. Farrell, W. M., Smith, P. H., Delory, G. T., Hillard, G. B., Marshall, J. R., Catling, D., ... & Cummer, S. A. (2004). Electric and magnetic signatures of dust devils from the 2000–2001 MATADOR desert tests. *Journal of Geophysical Research: Planets*, *109*(E3).

14. Farrell, W. M., Renno, N., Delory, G. T., Cummer, S. A., & Marshall, J. R. (2006). Integration of electrostatic and fluid dynamics within a dust devil. *Journal of Geophysical Research: Planets*, *111*(E1).

15. Farrell, W. M., McLain, J. L., Collier, M. R., & Keller, J. W. (2017). The Martian dust devil electron avalanche: Laboratory measurements of the E-field fortifying effects of dust-electron absorption. *Icarus*, *297*, 90-96.

16. Fedorova, A. A., Montmessin, F., Rodin, A. V., Korablev, O. I., Määttänen, A., Maltagliati, L., & Bertaux, J. L. (2014). Evidence for a bimodal size distribution for the suspended aerosol particles on Mars. *Icarus*, *231*, 239-260.

17. Fenton, L., Reiss, D., Lemmon, M., Marticorena, B., Lewis, S., & Cantor, B. (2016). Orbital observations of dust lofted by daytime convective turbulence. *Space Science Reviews*, *203*(1-4), 89-142.

18. Forward, K. M., Lacks, D. J., & Sankaran, R. M. (2009). Particle-size dependent bipolar charging of Martian regolith simulant. *Geophysical Research Letters*, *36*(13).

19. Freier, G. D. (1960), The electric field of a large dust devil, J. Geophys. Res., 65(10), 3504, doi:10.1029/JZ065i010p03504

20. Greeley, R., Balme, M. R., Iversen, J. D., Metzger, S., Mickelson, R., Phoreman, J., & White, B. (2003). Martian dust devils: Laboratory simulations of particle threshold. *Journal of Geophysical Research: Planets*, *108*(E5).

21. Greeley, R., Whelley, P. L., & Neakrase, L. D. (2004). Martian dust devils: Directions of movement inferred from their tracks. *Geophysical research letters*, *31*(24).

22. Greeley, R., Waller, D. A., Cabrol, N. A., Landis, G. A., Lemmon, M. T., Neakrase, L. D., ... & Whelley, P. L. (2010). Gusev Crater, Mars: Observations of three dust devil seasons. *Journal of Geophysical Research: Planets*, *115*(E7).

23. Guzewich, S. D., Toigo, A. D., Kulowski, L., & Wang, H. (2015). Mars Orbiter Camera climatology of textured dust storms. *Icarus*, *258*, 1-13.

24. Harrison, R. G., Barth, E., Esposito, F., Merrison, J., Montmessin, F., Aplin, K. L., ... & Houghton, I. M. P. (2016). Applications of electrified dust and dust devil electrodynamics to Martian atmospheric electricity. *Space Science Reviews*, 1-47.

25. Jackson, T. L., & Farrell, W. M. (2006). Electrostatic fields in dust devils: an analog to Mars. *IEEE Transactions on Geoscience and remote sensing*, *44*(10), 2942-2949.

26. Jackson, B., & Lorenz, R. (2015). A multiyear dust devil vortex survey using an automated search of pressure time series. *Journal of Geophysical Research: Planets*, *120*(3), 401-412.

27. Jemmett-Smith, B. C., Marsham, J. H., Knippertz, P., & Gilkeson, C. A. (2015). Quantifying global dust devil occurrence from meteorological analyses. *Geophysical research letters*, *42*(4), 1275-1282.

28. Kamra, A. K. (1972). Measurements of the electrical properties of dust storms. *Journal of Geophysical Research*, *77*(30), 5856-5869

29. Kunkel, W. B. (1950). The static electrification of dust particles on dispersion into a cloud. *Journal of Applied Physics*, *21*(8), 820-832.

30. Lacks, D. J., & Levandovsky, A. (2007). Effect of particle size distribution on the polarity of triboelectric charging in granular insulator systems. *Journal of Electrostatics*, *65*(2), 107-112.

31. Lorenz, R. D., & Lanagan, P. D. (2014). A barometric survey of dust-devil vortices on a desert playa. *Boundary-Layer Meteorology*, *153*(3), 555-568.

32. Lorenz, R. D., and B. K. Jackson, 2016. Dust Devil Populations and Statistics, Space Science Reviews, 10.1007/s11214-016-0277-9

33. Lorenz, R. D., 2016. Heuristic Estimation of Dust Devil Vortex Parameters and Trajectories from Single-Station Meteorological Data: Application to InSight at Mars, Icarus, 271, 326-337

34. Lorenz, R. D., Neakrase, L. D., Anderson, J. P., Harrison, R. G., & Nicoll, K. A. (2016). Point discharge current measurements beneath dust devils. *Journal of Atmospheric and Solar-Terrestrial Physics*, *150*, 55-60.

35. Malin, M. C., & Edgett, K. S. (2001). Mars global surveyor Mars orbiter camera: interplanetary cruise through primary mission. *Journal of Geophysical Research: Planets*, *106*(E10), 23429-23570.

36. Melnik, O., & Parrot, M. (1998). Electrostatic discharge in Martian dust storms. *Journal of Geophysical Research: Space Physics*, *103*(A12), 29107-29117.

37. McCarty, L. S., & Whitesides, G. M. (2008). Electrostatic charging due to separation of ions at interfaces: contact electrification of ionic electrets. *Angewandte Chemie International Edition*, *47*(12), 2188-2207.

38. Melnik, O., & Parrot, M. (1998). Electrostatic discharge in Martian dust storms. *Journal of Geophysical Research: Space Physics*, *103*(A12), 29107-29117.

39. Montabone, L., Marsh, K., Lewis, S. R., Read, P. L., Smith, M. D., Holmes, J., ... & Pamment, A. (2014). The Mars analysis correction data assimilation (MACDA) dataset V1. 0. *Geoscience Data Journal*, *1*(2), 129-139.

40. Murphy, J. R., & Nelli, S. (2002). Mars Pathfinder convective vortices: Frequency of occurrence. *Geophysical research letters*, *29*(23).

41. Murphy, J., Steakley, K., Balme, M., Deprez, G., Esposito, F., Kahanpää, H., ... & Patel, M. (2016). Field measurements of terrestrial and martian dust devils. *Space Science Reviews*, *203*(1-4), 39-87.

42. Neakrase, L. D. V., Balme, M. R., Esposito, F., Kelling, T., Klose, M., Kok, J. F., ... & Wurm, G. (2016). Particle lifting processes in dust devils. *Space Science Reviews*, *203*(1-4), 347-376.

43. Neubauer, F. M. (1966). Thermal convection in the Martian atmosphere. *Journal of Geophysical Research*, *71*(10), 2419-2426.

44. Ryan, J. A., & Lucich, R. D. (1983). Possible dust devils, vortices on Mars. *Journal of Geophysical Research: Oceans*, *88*(C15), 11005-11011.

45. Schofield, J. T., Barnes, J. R., Crisp, D., Haberle, R. M., Larsen, S., Magalhaes, J. A., ... & Wilson, G. (1997). The Mars Pathfinder atmospheric structure investigation/meteorology (ASI/MET) experiment. *Science*, *278*(5344), 1752-1758.

46. Sowinski, A., Miller, L., & Mehrani, P. (2010). Investigation of electrostatic charge distribution in gas–solid fluidized beds. *Chemical engineering science*, *65*(9), 2771-2781.

47. Stanzel, C., Pätzold, M., Williams, D. A., Whelley, P. L., Greeley, R., Neukum, G., & HRSC Co-Investigator Team. (2008). Dust devil speeds, directions of motion and general characteristics observed by the Mars Express High Resolution Stereo Camera. *Icarus*, *197*(1), 39-51.

48. Steakley, K., & Murphy, J. (2016). A year of convective vortex activity at Gale crater. *Icarus*, *278*, 180-193.

49. Thomas, P., & Gierasch, P. J. (1985). Dust devils on Mars. *Science*, *230*(4722), 175-177.

50. Trigwell, S., Grable, N., Yurteri, C. U., Sharma, R., & Mazumder, M. K. (2003). Effects of surface properties on the tribocharging characteristics of polymer powder as applied to industrial processes. *IEEE Transactions on Industry Applications*, *39*(1), 79-86.